Dynamical localization in nonideal kicked rotors

F. Revuelta,[1,2] R. Chacón,[3,4] and F. Borondo[2,5]

[1]*Grupo de Sistemas Complejos, Escuela Técnica Superior de Ingeniería Agronómica, Alimentaria y de Biosistemas, Universidad Politécnica de Madrid, Avda. Puerta de Hierro 2-4, 28040 Madrid, Spain*

[2]*Instituto de Ciencias Matemáticas (ICMAT), Cantoblanco, 28049 Madrid, Spain*

[3]*Departamento de Física Aplicada, Escuela de Ingenierías Industriales, Universidad de Extremadura, Apartado Postal 382, E-06006 Badajoz, Spain*

[4]*Instituto de Computación Científica Avanzada (ICCAEx), Universidad de Extremadura, E-06006 Badajoz, Spain*

[5]*Departamento de Química, Universidad Autónoma de Madrid, Cantoblanco, 28049 Madrid, Spain*

(Received 20 July 2018; published 4 December 2018)

We discuss a general useful theoretical framework to study dynamical localization in ultracold atomic systems confined in periodically shaken optical lattices. Our theory allows to understand some limitations of the usual approach concerning prototypical δ-kicked systems, as well as to explain the experimental results for which finite-time effects cannot be neglected. Specifically, we predict that the strength of dynamical localization reaches a maximum as a function of the width of the pulsatile modulation, whenever its amplitude and period satisfy a given relationship. Additionally, we describe a quite simple scenario for the quantum suppression of classical diffusion, which is confirmed by extensive numerical simulations: The activation of Heisenberg's uncertainty principle giving rise to a drastic reduction of the quantum momentum dispersion if, and only if, the classical dynamics is sufficiently chaotic.

DOI: 10.1103/PhysRevE.98.062202

I. INTRODUCTION

The quantum suppression of classical diffusion, usually known as dynamical localization (DL) for short [1,2], is a fascinating phenomenon that has attracted wide attention in the physics community since its first experimental observation by Graham *et al.* [3], partly due to its relevance in many fields. Thus, DL provides an excellent benchmark to test the classical-quantum correspondence in classically chaotic systems [4], a situation where the solid support provided by semiclassical theories [5], such as the Wentzel-Kramers-Brillouin or the Einstein-Brillouin-Keller quantization schemes, dramatically fails due to the widespread destruction of invariant tori. Also, DL is strongly related to Anderson localization (in space), which describes the metal-insulator transition for disordered systems [6,7]. Recently, Garreau [8] has demonstrated the feasibility of considering DL as a quantum simulator to study this interesting phenomenon in ultracold atoms (UCAs).

The standard theoretical approach to DL heavily relies on the ideal δ-kicked rotor model [9–14], where the modulation pulses are chosen to be infinitely narrow. The reason of this choice is clear: This paradigmatic model has a well understood classical limit (the Chirikov-Taylor or standard map [15]) and the corresponding quantum dynamics can also be straightforwardly studied due to the simple analytical character of the associated quantum evolution operator. The ability of this mathematical model to accurately describe actual experiments [3,4,16–18], in which finite-time effects cannot be neglected, is limited. Despite this limitation, little effort has been made to the development of more elaborated nonideal theoretical models [19–21] that take into account the effects of finite-width time pulses. Note that, contrary to what happens for the kicked rotor, these models do not have an analytical solution, and then they have to be studied numerically.

In an attempt to overcome this difficulty and to establish a better understanding of actual experimental findings, we develop in this paper a new theoretical approach to accurately describe the dynamics of a cloud of UCAs trapped in a periodically shaken optical lattice. This system has been experimentally studied [3,4] by confining a gas of UCAs in an standing-wave lattice created by two opposite mirrors with a modulating device, such as a moving piezoelectrical cristal. Traditionally, DL has been systematically controlled in this kind of system by tuning only the amplitude [22].

We also demonstrate that a better, yet optimum, control of DL can be achieved in a more general fashion by also changing the modulation's waveform and period. For this purpose, we replace the δ-function with a more general pulse function [see definition in Eq. (2) below]. The specific waveform of this function can be changed by solely tuning a single parameter, and its functional form permits to obtain analytical expressions for some of the main quantities involved in our analysis.

The organization of the paper is as follows. In Sec. II we briefly present the system of UCAs driven by finite pulses, paying special attention to the definition of our modulation function. In Sec. III we discuss the numerical methods used to study the DL at the classical and quantum level, and the analytical method used to evaluate the width of the classical stochastic layer by using Melnikov's method. In Sec. IV we present and discuss the results obtained in this work. Finally, we conclude with Sec. V by summarizing our conclusions and discussing future work.

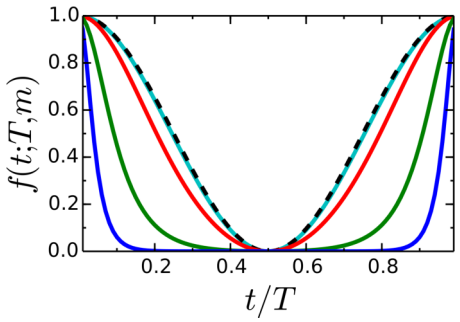

FIG. 1. Waveform of the pulsatile modulation, which is varied by solely changing a single parameter, m, from a cosine squared form when $m = 0$ (dashed black line) to a periodic sharply kicking modulation very close to the periodic δ-function, but with finite amplitude and width, when $m \simeq 1$. The waveforms corresponding to $m = 0.2$ (cyan line), $m = 0.6$ (red line), $m = 0.99999$ (green line), and $m = 1\text{–}10^{-14}$ (blue line) are shown.

II. MODEL SYSTEM WITH FINITE PULSES

The system that we study is formed by a ensemble of non-interacting UCAs confined in a periodically driven optical lattice. As the particles have no correlations, their motion can be suitably described by the mass-scaled spatial-periodic one-particle Hamiltonian

$$\mathcal{H}(p,x,t) = \frac{p^2}{2} - Ff(t;T,m)\,\cos x, \tag{1}$$

where we choose the periodic modulation function $f(t;T,m)$ that accounts for the interaction with the external field, as

$$f(t;T,m) \equiv \frac{dn[2K(m)t/T;m] - \sqrt{1-m}}{1-\sqrt{1-m}}, \tag{2}$$

where T is the period, $m \in [0,1]$ is the shape parameter controlling the modulation waveform, $K(m)$ is the complete elliptic integral of first kind, and dn$(\cdot;$m$)$ is a Jacobian elliptic function [24] of parameter m. Some waveforms of $f(t;T,m)$ are shown in Fig. 1 for several values of m. As can be seen, in the $m = 0$ limit, the pulses have a cosine squared form, $f(t;T,m=0) = \cos^2(\pi t/T)$, being maximum the width of the pulse [25]. In this limiting case, the Hamiltonian (1) mimics a parametrically and sinusoidally perturbed nonlinear pendulum. As the value of m increases, the effective width of the pulses slowly decreases over the range $0 \leqslant m \leqslant 0.9$. Also, the effective width changes dramatically for larger values of m. Thus, the pulse width reduces ∼50% when the shape parameter changes from $m = 0.99999$ (green line in Fig. 1) to $m = 1\text{–}10^{-14}$ (blue line in Fig. 1). The pulse vanishes in the limit $m \to 1$, a situation where the system is no longer driven. However, in this limit, our model tends to the paradigmatic kicked rotor [9–14] when the amplitude F is simultaneously increased in such a way that the transmitted impulse remains constant. Moreover, the specific form of the finite width pulse (2) permits to obtain analytical expressions for some of the main quantities involved in this work. Thus, Hamiltonian (1) provides a single model which is able to describe both real-world experimental finite-duration pulses as well as the limiting case of a free rotor through a soft transition by solely tuning the shape parameter m.

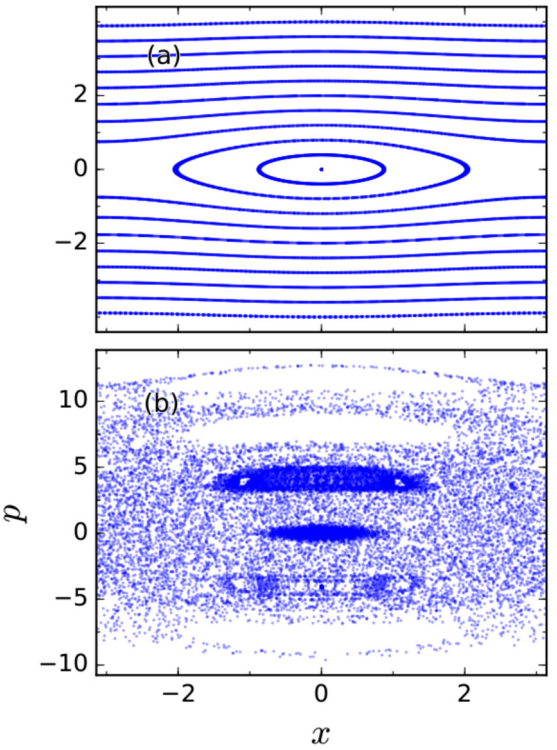

FIG. 2. The pulsatile modulation can make the motion of the trapped atoms regular or chaotic depending upon the values chosen for their parameters F, T, m, as shown by the stroboscopic Poincaré surfaces of section computed for (a) $m = 0.99999$, $F = 1$, $T = 1$, and (b) $m = 0.99999$, $F = 5$, $T = 10$. See the Supplemental Material [23] for additional examples.

To understand the classical dynamical characteristics of our system for different pulsatile modulations, we show two examples of typical pictures of its phase space in Fig. 2. For this purpose, we used stroboscopic Poincaré maps, consisting of the (x, p) when time t is a multiple of the period T, i.e., $t = kT$ with $k \in \mathbb{Z}^+$, obtained from classical trajectories sampling all accessible phase space.

As can be seen, in Fig. 2(a), corresponding to $m = 0.99999$, $F = 1$, $T = 1$, the motion of the particles is confined into well-defined ellipses or circles, indicating the existence of non-destroyed invariant tori, while in Fig. 2(b), corresponding to $m = 0.99999$, $F = 5$, $T = 10$, the coordinates are delocalized over all the available phase space, due to a widespread breakdown of the classical structures, as dictated by the Kolmogorov-Arnold-Moser (KAM) theorem [15], thus opening a route to chaos. Additional examples of stroboscopic maps are shown in Figs. S.1, S.2, and S.3 of the Supplemental Material [23].

These results clearly indicate that the onset of chaos gives rise to the possibility of DL, which is a purely quantum phenomenon that happens when the system exhibits a classically chaotic motion. The degree of chaoticity is well characterized in terms of the extent, i.e., the width of the stochastic layer, which can be analytically calculated in the case of our modulation function. Notably, our extensive numerical simulations, discussed in Sec. IV, indicate that the strength of DL is maximum when the width of the chaotic layer is also maximum.

This fascinating connection can shed new light on the emergence of DL. In other words, Heisenberg's uncertainty principle seems to constitute a limit for the dispersion of the quantum momentum distribution, while having no effect on its classical counterpart. This issue will be discussed in detail in Sec. V.

III. METHOD

A. Numerical calculations

The classical momentum dispersion is computed by numerically solving the Liouville equation

$$[\partial_t + p\partial_x - Ff(t;T,m)\ \sin x]\ P(x,\,p;t) = 0, \qquad (3)$$

using a standard fourth-order Runge-Kutta method [26] with periodic boundary conditions $P(x+L,\,p;t) = P(x,\,p;t)$, $L = 2n\pi$ with L the size of the quantization box, and $n \in \mathbb{Z}^+$. The classical momentum distribution is then calculated as $P_C(p,t) = \int P(x,\,p;t)\,dx$, where $P(x,\,p;t)$ is the evolution of a uniform distribution of 2×10^4 trajectories launched over one wavelength following initially a Gaussian momentum distribution with a width of $\Delta p_0 = 0.386$ (cf. Refs. [4,16,21,27]) up to 320 units of time.

The corresponding quantum momentum distributions, $P_Q(p,t)$, have been calculated by averaging the time-evolution of a localized wave packet

$$\psi(x,\,t=0) = (\pi\,\Delta x_0)^{-1/4}\exp\left[-\frac{(x-x_0)^2}{2\Delta x_0} + \frac{ixp_0}{\hbar_{\rm eff}}\right], \quad (4)$$

centered at $x_0 \in [0,\,L]$ with $p_0 = 0$ and $\Delta x_0 = \hbar_{\rm eff}/\Delta p_0$, being $\hbar_{\rm eff} \equiv 2\hbar k^2 T/(\pi M)$ the effective Planck constant, where M is the atomic mass, and k the wave number. The parameter $\hbar_{\rm eff}$ plays the role of Planck's reduced constant for the scaled Hamiltonian (1), and then characterizes the "quanticity" of the system, as the scaled operators $\hat{x}$ and $\hat{p}$ fulfill Heisenberg's uncertainty relation defined as $[\hat{x},\,\hat{p}] = i\hbar_{\rm eff}$. Notice the dependence of $\hbar_{\rm eff}$ on the time period, T, which is a consequence of the dependence of the scaled momentum, p, on the scaled time (see Refs. [4,21] for further details).

The time-evolution of wave-packet (4) is performed by numerically solving the usual time-dependent Schrödinger equation

$$i\ \hbar_{\rm eff}\ \partial_t\psi = -\left[\frac{\hbar_{\rm eff}^2}{2}\partial_{xx}^2 + Ff(t;T,m)\ \cos x\right]\psi, \quad (5)$$

which is numerically solved using a fast Fourier [26] transform method up to 320 units of time, as in the classical calculations. Let us remark that this time is sufficiently long to observe DL, even for the largest period considered here, $T = 10$, for which only 32 modulation cycles took place. It is worth noting that Lignier *et al.* observed DL by using a time propagation of solely 20 cycles (see Fig. 3 in Ref. [12]).

B. Melnikov analysis of the stochastic layer width

Firstly, this subsection briefly describes Melnikov's method [15,28,29] for the simple case of a perturbed integrable Hamiltonian system with one degree of freedom. Consider the system

$$\dot{\mathbf{x}} = h_0(\mathbf{x}) + \varepsilon h_1(\mathbf{x},\,t),$$
$$\mathbf{x} = (x_1,\,x_2), \qquad (6)$$

where the unperturbed system ($\varepsilon = 0$) is an integrable Hamiltonian system which possesses a hyperbolic fixed point X_0 and a separatrix orbit $x_0(t)$ such that $\lim_{t\to\pm\infty} x_0(t) = X_0$, while the stable and unstable manifolds $x^s(t)$, $x^u(t)$ smoothly join. In general, the perturbation term h_1 which is T-periodic in time, can introduce dissipation and non-autonomous excitation. For $\varepsilon \neq 0$, the (now) perturbed stable and unstable manifolds no longer join smoothly such that, if the ratio of dissipation and excitation is sufficiently small, the stable and unstable manifolds will intersect transversally, creating a homoclinic point. This process is called a homoclinic bifurcation and indicates the onset of chaotic instabilities. To check when a transverse crossing occurs, Melnikov introduced a function $M(t')$ (now known as the Melnikov function) which measures the distance between the perturbed stable and unstable manifolds in the Poincaré surface section as

$$M(t') \equiv \int_{-\infty}^{\infty} h_0(x_0(t-t')) \wedge h_1(x_0(t-t'),\,t)\,dt, \qquad (7)$$

where $\wedge$ is the wedge operator ($\mathbf{x}\wedge\mathbf{y} = x_1y_2 - x_2y_1$). If the Melnikov function presents a simple zero, the manifolds intersect transversally and chaotic instabilities result. When h_1 is a Hamiltonian perturbation, this leads to the appearance of an unstable layer—meaning the possibility of persistent chaotic motion—along the separatrix of the unperturbed system. The width Δ of this chaotic separatrix layer can be estimated from the Melnikov function [15,28,29] as

$$\Delta = \left|\frac{\max_{t'} M(t')}{|h_0[x_0(0)]|}\right| + \mathcal{O}(\varepsilon^2). \qquad (8)$$

Secondly, we calculated the width of the chaotic layer, $d(T,\,F,\,m)$, associated with Eq. (1) by assuming that the integrable pendulum $\ddot{x} + F\sin x = 0$ corresponds to $h_0(\mathbf{x})$, while $F[1 - f(t;T,m))]\sin x$ plays the role of the perturbative term $h_1(\mathbf{x},\,t)$ as

$$d(T,\,F,\,m) \equiv \frac{1}{2}\max_{t_0}\ M(t_0)$$
$$= \frac{4\pi^3}{T^2}\sum_{n=1}^{\infty} n^2\ c_n(m)\ b_n(T,\,F), \qquad (9)$$

where

$$b_n(m,\,T,\,F) = \mathrm{csch}\left(\frac{\mathrm{n}\pi^2}{\mathrm{T}\sqrt{\mathrm{F}}}\right),$$
$$c_n(m) = \frac{\pi\ \mathrm{sech}[\mathrm{n}\pi\mathrm{K}(1-\mathrm{m})/\mathrm{K}(\mathrm{m})]}{(1-\sqrt{1-m}\ )\ K(m)}. \qquad (10)$$

From the expression (9) for the width, one readily obtains

$$\lim_{F\to0} d(T,\,F,\,m) = \lim_{T\to0} d(T,\,F,\,m) = \lim_{m\to1} d(T,\,F,\,m) = 0,$$
$$\lim_{m\to0} d(T,\,F,\,m) = \frac{2\pi^3}{T^2}\ \mathrm{csch}\left(\frac{\pi^2}{\mathrm{T}\sqrt{\mathrm{F}}}\right). \qquad (11)$$

IV. RESULTS

In this section we discuss the results obtained for DL in our system, which is derived from the Hamiltonian model (1). DL is evaluated by comparing the classical and quantum momentum distributions obtained by solving the corresponding equations of motion (see Sec. III A). Specifically, we calculated the difference between the classical and quantum dispersions

$$\Delta p_{C-Q} = \Delta p_C - \Delta p_Q,$$
$$\Delta x_{C-Q} = \Delta x_C - \Delta x_Q, \tag{12}$$

being $\Delta p_C = (\langle p_C^2\rangle - \langle p_C\rangle^2)^{1/2}$, $\Delta p_Q = (\langle p_Q^2\rangle - \langle p_Q\rangle^2)^{1/2}$, $\Delta x_C = (\langle x_C^2\rangle - \langle x_C\rangle^2)^{1/2}$, and $\Delta x_Q = (\langle x_Q^2\rangle - \langle x_Q\rangle^2)^{1/2}$, respectively.

A. Dependence of DL on the modulation amplitude and waveform

In Figs. 3(a)–3(c) we show the classical and quantum momentum distributions dispersions, $\Delta p_{C,Q}$, and their difference $\Delta p_{C-Q} = \Delta p_C - \Delta p_Q$, as a function of the modulation strength, F, and shape parameter, m, for a constant value of the period $T = 1$. Notice that the color scales used have been made homogeneous (just to guide the eye) since the dispersion ranges are quite different. Specifically, the dispersion varies between 4 and 70 for the classical results, and between 1.5 and 15 for the quantum ones (see Supplemental Material [23]). As can be seen, the overall behavior is such that these three quantities increase as both F and m are increased. Also, notice that the behavior of Δp_{C-Q} qualitatively follows that of the analytically evaluated width of the stochastic layer, $d(T, F, m)$ [cf. Eq. (9)], which is shown for comparison in Fig. 3(d). A similar agreement is found for other values of the period, as in the cases shown in Figs. 3(e) and 3(f) corresponding to $T = 10$. (See also Figs. S.4, S.5, and S.6 of the Supplemental Material [23].)

Remarkably, this agreement holds even in the limit of narrow pulses ($m \lesssim 1$), where $d(T, F, m)$ is expected to exhibit a maximum as a function of m when the amplitude is larger than a critical value, F_c, which in turn decreases with the period (cf. Sec. III B). For example, we have that $F_c(T = 1) \simeq 7$, being the corresponding maximum in the momentum difference, $\Delta p_{C-Q}|_{\max}$, localized at $m_{\max} \simeq 0.84$, while for $F_c(T = 5) \simeq 0.4$ it is found that $m_{\max} \simeq 0.95$.

Figure 3(g) shows the dependence of Δp_{C-Q} on the shape parameter m for $F = 30$ and $F = 40$, corresponding, respectively, to the green and red lines in panel (c). Indeed, Fig. 3(g) shows that the maximum of Δp_{C-Q}, and hence the maximum strength of DL, increases as the amplitude is increased from $F = 30$ ($\Delta p_{C-Q}|_{\max} \simeq 58.6$) to $F = 40$ ($\Delta p_{C-Q}|_{\max} \simeq 70.2$). Moreover, the corresponding maximum, $m_{\max}$, increases as the amplitude is increased: from $m_{\max} \simeq 0.9992$ at $F = 30$ to $m_{\max} \simeq 1\text{–}10^{-7}$ at $F = 40$, thus mimicking the (same) behavior of the width $d(T, F, m)$, which is also shown in dashed lines in the respective insets.

Also, Fig. 3(h) shows the dependence of $\Delta p_{C-Q}|_{\max}$ on the amplitude, for six values of the period. Notice the lack of data points for small values of F and T, which is due to the absence of any maximum in such ranges. Although DL is

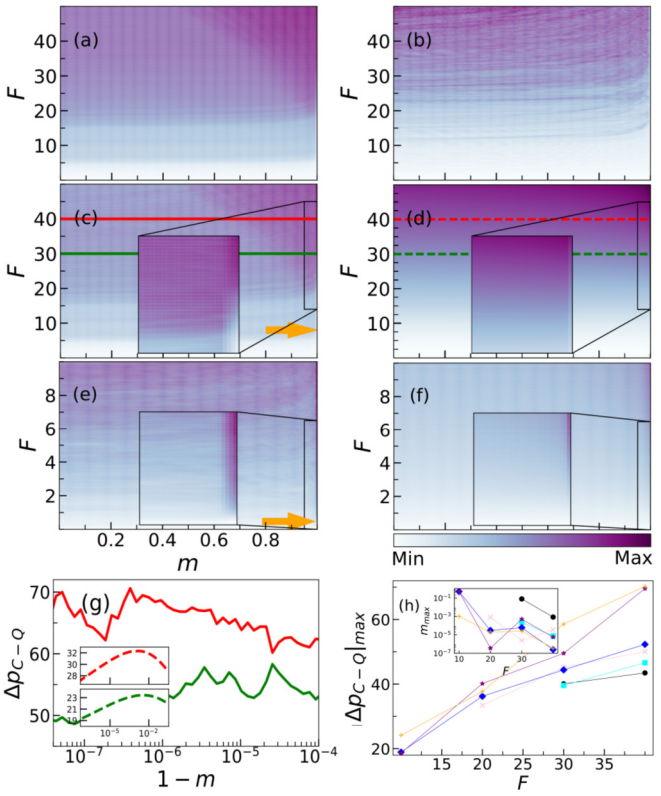

FIG. 3. Comparison between the strengths of chaos and dynamical localization in the parameter plane $m - F$. (a) Classical momentum dispersion, Δp_C, (b) quantum momentum dispersion, Δp_Q, and (c) difference, $\Delta p_{C-Q} \equiv \Delta p_C - \Delta p_Q$, as a function of the amplitude F and shape parameter m for $T = 1$. The inset show the parametric region where maxima occur. (d) Width of the stochastic layer $d(T = 1, F, m)$ [cf. Eq. (9)]. The yellow arrows indicate the values of the critical amplitude, F_c, which have to be overcome for the appearance of the maxima. (e) and (f): Same as (c) and (d), respectively, for $T = 10$. (g) Difference Δp_{C-Q} for $T = 1$ as a function of the shape parameter m for two values of the amplitude [also shown as horizontal lines in (c) and (d)]: $F = 30$ (bottom green lines) and $F = 40$ (top red lines). The insets show the respective analytical estimates [cf. Eq. (9)] of the stochastic layer widths as functions of the shape parameter. (h) Maximum values of the difference Δp_{C-Q} and respective maxima $m_{\max}$ (inset) as a function of the amplitude F for six values of the period: $T = 0.5$ (black circle), 0.6 (cyan square), 0.7 (pink x cross), 0.8 (blue diamond), 0.9 (purple asterisk), and 1.0 (orange plus symbol).

an interference effect, all these results suggest that the origin of DL is found in the chaotic behavior of the classical limit. The inset in the figure shows the value of the shape parameter, $m_{\max}$, where $\Delta p_{C-Q}|_{\max}$ is found for the same parameters of the main panel. As already mentioned, the value of $m_{\max}$ tends to 1 as F and/or T increase.

B. Dependence of DL on the modulation period and waveform

Figures 4(a) and 4(c) show Δp_{C-Q} as a function of the period T and the shape parameter m for two values of the amplitude: $F = 1$ and $F = 10$, respectively (see also Figs. S.7, S.8, and S.9 of the Supplemental Material [23]). The corresponding values for the stochastic layer width $d(T, F, m)$

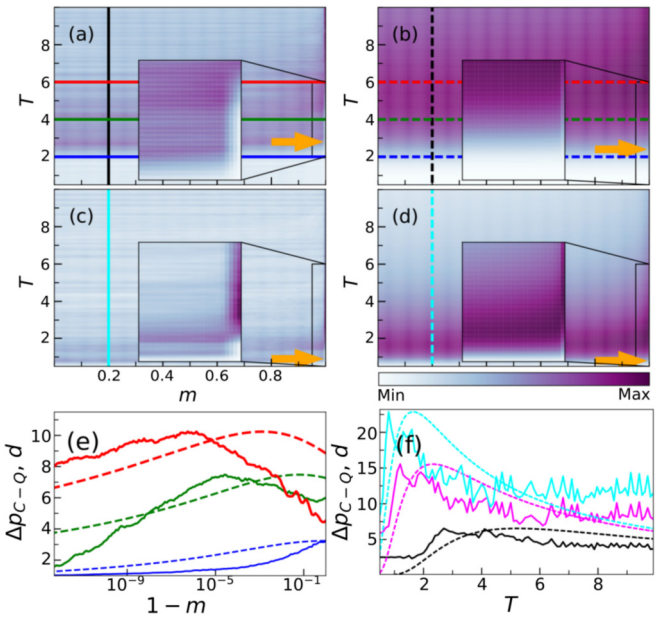

FIG. 4. Comparison between the strengths of chaos and dynamical localization in the parameter plane $m - T$. (a), (c) Difference between the classical and quantum momentum dispersions, $\Delta p_{C-Q} \equiv \Delta p_C - \Delta p_Q$, and (b), (d) stochastic layer width, $d(T, F, m)$, as a function of the period T and the shape parameter m for two values of the amplitude: (a), (b) $F = 1$ and (c), (d) $F = 10$. The insets show the parameter regions where the respective maxima occur. The yellow arrows indicate the values of the critical period, T_c, which have to be overcome for the appearance of such maxima. (e) Δp_{C-Q} (solid lines) and $d(T, F = 1, m)$ (dashed lines) as functions of the shape parameter m, for $F = 1$ and three values of the period [also shown as horizontal lines in (a) and (b)]: $T = 2$ (bottom blue lines), $T = 4$ (medium green lines), and $T = 6$ (top red lines). (f) Δp_{C-Q} (solid lines) and $d(T, F, m)$ (dashed lines) as a function of the period T for $m = 0.2$ and three values of the amplitude: $F = 1$ (bottom black lines [also shown as vertical lines in (a) and (b)]), $F = 5$ (medium magenta lines [also shown as vertical lines in (c) and (d)]), and $F = 10$ (top cyan lines).

[cf. Eq. (9)] are shown in Figs. 4(b) and 4(d), respectively. As can be seen, both quantities, and hence the strength of DL, increase as the amplitude is increased. Moreover, they exhibit maxima as a function of T for a given value of the shape parameter m, being these maxima very close to each other. Also, and as predicted from the analysis of the stochastic layer width $d(T, F, m)$ (cf. Sec. III B), these maxima only appear when the period exceeds a critical value, T_c, values which are indicated with a yellow arrow in each panel. The value of $T_c(F)$ decreases with the modulation amplitude. For example, we have that $T_c(F = 1) \simeq 2.7$, being the corresponding maximum in the momentum difference, $\Delta p_{C-Q}|_{\max}$, localized at $m_{\max} \simeq 0.50$, while for $T_c(F = 5) \simeq 1.2$ it is found that $m_{\max} \simeq 0.85$.

The exact values of these maxima are more clearly seen when the quantities are plotted as a function of only one of the parameters, either m or T, as it is shown in Figs. 4(e) and 4(f), respectively. For the sake of comparison, the results for $F = 5$ have been added in Fig. 4(f). To get a clearer comparison with Δp_{C-Q}, the values of the width $d(T, F, m)$

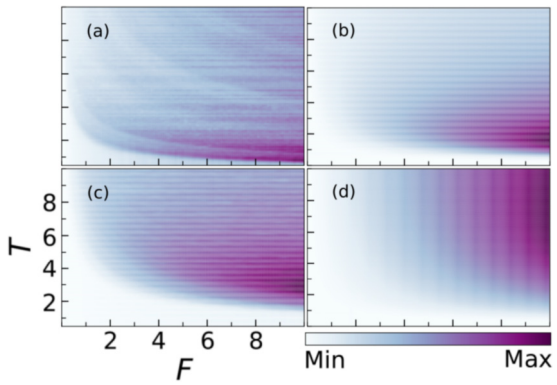

FIG. 5. (a), (b) Difference between the classical and quantum momentum dispersions, $\Delta p_{C-Q} \equiv \Delta p_C - \Delta p_Q$, and (c), (d) corresponding stochastic layer width, $d(T, F, m)$, as a function of the period T and the amplitude F for two values of the shape parameter: (a), (c) $m = 0$, and (b), (d) $m = 1$–10^{-14}.

has been suitably scaled in Fig. 4(e). Notice the absence of a maximum for $F = 1$ and $T = 2$ (dark blue curve), due to the fact that this value of the period is below the corresponding threshold $T_c(F = 1) \simeq 2.8$, while the appearance of a maximum is observed at the same value of the period when the amplitude is sufficiently increased, i.e., $T > T_c(F)$ [cf. inset of Fig. 4(c)]. Moreover, the values of these maxima tend to accumulate very near $m = 1$ as T is increased, as shown for the values $T = 4$ and $T = 6$ (red and green lines, respectively) in Fig. 4(e). Additionally, the quantities Δp_{C-Q} and $d(T, F, m)$ also exhibit maxima as a function of T, at certain values $T = T_{\max}$ while keeping constant the amplitude and shape parameter. Some illustrative examples are shown in Fig. 4(f), where it is seen that these quantities increase as the amplitude F is increased. The values $T_{\max}$ decrease as the amplitude is increased. It is worth noticing that due to the very different nature of the quantities Δp_{C-Q} and $d(T, F, m)$, the expected agreement between the corresponding $T_{\max}$ is only qualitative.

C. Revisiting the traditional way of controlling DL

As already mentioned in Sec. I, DL has been traditionally controlled by changing the values of the amplitude F and the period T of the driving field. However, our present findings clearly demonstrate the great controlling potential of the modulation waveform. Accordingly, we propose in the present paper that an alternative and very efficient way of controlling DL is by tuning the modulation waveform in our generalized model. Remarkably, this is achieved by solely changing a single parameter, namely, the shape parameter m, while the waveform of our modulating field allows to reliably describe experimental situations.

To systematically establish the influence of the modulation waveform in the DL control, we show the values of Δp_{C-Q} as a function of the amplitude F and the period T in Fig. 5, for two limiting values of the shape parameter: $m = 0$ [cf. Fig. 5(a)], which corresponds to a cosine squared form, and $m = 1$–10^{-14} [cf. Fig. 5(c)], for which the controlling pulse is very narrow, but still finite. Similarly to the

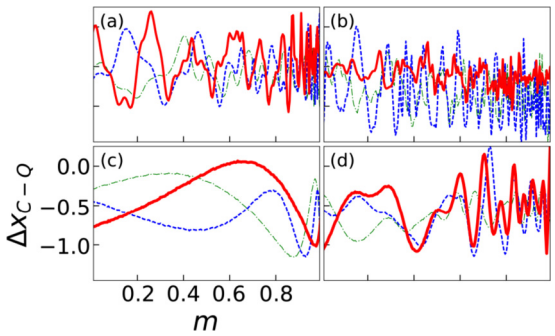

FIG. 6. Difference between the classical and quantum position dispersions, $\Delta x_{C-Q} = \Delta x_C - \Delta x_Q$, as a function of the shape parameter m for three values of the effective Planck constant $\hbar_{\text{eff}} = 0.72$ (thick continuous red lines), 0.36 (dashed blue lines), and 0.18 (thin dotted-dashed green lines), respectively, and (a) $T = 1$, $F = 10$, (b) $T = 1$, $F = 40$, (c) $T = 10$, $F = 0.5$, and (d) $T=10$, $F = 4$.

aforementioned discussed examples, the results for $d(T, F, m)$ agree remarkably well with those corresponding to Δp_{C-Q} for the same parameter values [cf. Figs. 5(b) and 5(d), respectively]. Note that no substantial DL occurs if either T or F are sufficiently small. Also, it is found again that, for a fixed value of the amplitude F, there exists a value of the period T for which the DL strength is maximum, similarly to which it was already discussed in relation to the results in Fig. 4(f). Figures S.10 to S.15 of the Supplemental Material [23] report other examples obtained for different values of the modulation waveform.

V. SUMMARY AND OUTLOOK

In the present work, we have introduced a new theoretical model to study DL, which takes into account the finite nature of real-world pulses, a feature which is not included in the traditional δ-kicked rotor model.

Our results indicate that there exists a deep correlation between the strengths of chaos and DL (quantified respectively by means of the stochastic layer width, d, and the difference between the classical and quantum momentum dispersions, Δp_{C-Q}) over the entire parameter space (amplitude F, period T, and shape parameter m) of the pulse function.

Specifically, we have demonstrated that the strengths of chaos and DL exhibit a maximum value as a function of the shape parameter, a relevant property that can be used to tune DL to its maximal value by controlling the chaos strength. For a fixed period (amplitude), this maximum is theoretically predicted and numerically observed only when the amplitude (period) exceeds a certain critical value of $F_c(T)$ [$T_c(F)$]. These critical values decrease with T and F, respectively. Furthermore, we have demonstrated that the strengths of chaos and DL also exhibit a maximum value as a function of the period when keeping constant the remaining parameters.

Finally, we would like to address another important point. In sharp contrast to the behavior of Δp_{C-Q}, the difference Δx_{C-Q} seems to be relatively insensitive to changes in both the modulation parameters, F, T, m, and the "quanticity" of the system, $\hbar_{\text{eff}}$, as shown in Fig. 6. Also, it is found that the obtained range of values of Δx_{C-Q} suggest that $\Delta x_Q \sim \Delta x_C$, irrespective of the values of the above mentioned parameters. Notice that, for all parameters considered in Fig. 6, $|\Delta x_{C-Q}| \lesssim 1.5$, while the Δp_{C-Q} is defined in a much wider range, as inferred from inspection of Figs. S.4(c)–S.15(c) of the Supplemental Material [23], where it is shown that Δp_C is up to five times larger than Δp_Q [compare panels (a) and (b) of Figs. S.4–S.15 of the Supplemental Material [23]]. In light of this result, the Heisenberg's uncertainty relation $\Delta x_Q \Delta p_Q \geqslant \hbar_{\text{eff}}/2$ should be rewritten as

$$\Delta p_Q \gtrsim \frac{\hbar_{\text{eff}}}{2\Delta x_C}. \tag{13}$$

The key point here is that the strength of the classical dispersion ultimately depends on the chaos strength, while we have shown that the latter can be effectively quantified by estimating the width of the stochastic layer. Equation (13) provides a simple explanation of the origin of DL: it appears due to the unavoidable activation of the Heisenberg's uncertainty principle as $\hbar_{\text{eff}}$ increases from 0 (classical limit) to the deep quantum regime ($\hbar_{\text{eff}}$ high), through the semiclassical regime ($\hbar_{\text{eff}} \gtrsim 0$), by proportionally limiting the quantum momentum dispersion when the system is classically chaotic. While the strict equality in Eq. (13) applies only in the case of a coherent wave packet moving in a harmonic potential, our results indicate that this seems to be also true in the present case. To the best of our knowledge, there is no formal justification of this fascinating behavior, which certainly deserves further investigation due to its fundamental relevance. We expect that this result can stimulate experimental work to clarify the subtleties of DL in real-world systems subject to periodic pulses of finite width.

ACKNOWLEDGMENTS

This work has been partially supported by the Spanish Ministry of Economy and Competitiveness (ES) under Contracts No. MTM2015-63914-P and Severo Ochoa Contract No. SEV-2015-0554. R.C. gratefully acknowledges financial support from the Junta de Extremadura (JEx, Spain) through Project No. GR18081, and F.R. the financial support of the Programa Propio of the Universidad Politécnica de Madrid.

[1] I. Guarneri, G. Casati, and V. Karle, Phys. Rev. Lett. **113**, 174101 (2014).
[2] L. E. Reichl, *The Transition to Chaos. Conservative Classical Systems and Quantum Manifestations* (Springer, New York, 1994).
[3] R. Graham, M. Schlautmann, and D. L. Shepelyansky, Phys. Rev. Lett. **67**, 255 (1991).
[4] F. L. Moore, J. C. Robinson, C. Bharucha, P. E. Williams, and M. G. Raizen, Phys. Rev. Lett. **73**, 2974 (1994).
[5] M. Brack and R. K. Bhaduri, *Semiclassical Physics* (Addison-Wesley, Reading, MA, 1997).
[6] P. W. Anderson, Phys. Rev. **109**, 1492 (1958).
[7] S. Fishman, D. R. Grempel, and R. E. Prange, Phys. Rev. Lett. **49**, 509 (1982).

[8] J.-C. Garreau, C. R. Phys. **18**, 31 (2017), Prizes of the French Academy of Sciences 2015 / Prix de l'Academie des Sciences 2015.
[9] H. Ammann, R. Gray, I. Shvarchuck, and N. Christensen, Phys. Rev. Lett. **80**, 4111 (1998).
[10] C. F. Bharucha, J. C. Robinson, F. L. Moore, B. Sundaram, Q. Niu, and M. G. Raizen, Phys. Rev. E **60**, 3881 (1999).
[11] G. Abal, R. Donangelo, A. Romanelli, A. C. Sicardi Schifino, and R. Siri, Phys. Rev. E **65**, 046236 (2002).
[12] H. Lignier, J. C. Garreau, P. Szriftgiser, and D. Delande, Europhys. Lett. **69**, 327 (2005).
[13] J. Chabé, H. Lignier, H. Cavalcante, D. Delande, P. Szriftgiser, and J. C. Garreau, Phys. Rev. Lett. **97**, 264101 (2006).
[14] M. Bitter and V. Milner, Phys. Rev. Lett. **118**, 034101 (2017).
[15] A. J. Lichtenberg and M. A. Lieberman, *Regular and Chaotic Dynamics*, Applied Mathematical Sciences (Springer, Berlin, Heidelberg, 2010).
[16] R. Graham, M. Schlautmann, and P. Zoller, Phys. Rev. A **45**, R19 (1992).
[17] J. Ringot, P. Szriftgiser, J. C. Garreau, and D. Delande, Phys. Rev. Lett. **85**, 2741 (2000).
[18] D. A. Steck, W. K. Oskay, and M. G. Raizen, Science **293**, 274 (2001).
[19] P. J. Bardroff, I. Bialynicki-Birula, D. S. Krähmer, G. Kurizki, E. Mayr, P. Stifter, and W. P. Schleich, Phys. Rev. Lett. **74**, 3959 (1995).
[20] R. Chacón, F. Borondo, and D. Farrelly, Europhys. Lett. **86**, 30004 (2009).
[21] F. Revuelta, R. Chacón, and F. Borondo, Europhys. Lett. **110**, 40007 (2015).
[22] S. van Frank, M. Bonneau, J. Schmiedmayer, S. Hild, C. Gross, M. Cheneau, I. Bloch, T. Pichler, A. Negretti, T. Calarco, and S. Montangero, Sci. Rep. **6**, 34187 (2016).
[23] See Supplemental Material at http://link.aps.org/supplemental/10.1103/PhysRevE.98.062202 for further examples of Poincaré surfaces of section, classical and quantum momentum distributions and their differences, and chaotic layer widths.
[24] M. Abramowitz and I. Stegun, *Handbook of Mathematical Functions* (Dover Publications, Mineola, NY, 1965).
[25] R. Chacón and A. M. García-Hoz, Phys. Lett. A **281**, 231 (2001).
[26] W. H. Press, S. A. Teukolsky, W. T. Vetterling, and B. P. Flannery, *Numerical Recipes 3rd Edition: The Art of Scientific Computing* (Cambridge University Press, New York, 2007).
[27] R. Chacón, Europhys. Lett. **77**, 30001 (2007).
[28] J. Guckenheimer and P. Holmes, *Nonlinear Oscillations, Dynamical Systems, and Bifurcations of Vector Fields*, Applied Mathematical Sciences (Springer, New York, 2002).
[29] S. Wiggins, *Chaotic Transport in Dynamical Systems*, Interdisciplinary Applied Mathematics (Springer-Verlag, Berlin, 1992).